CMS Physics Analysis Summary

Contact: cms-pag-conveners-exotica@cern.ch 2018/06/01

Search for long-lived particles with displaced vertices in multijet events in proton-proton collisions at $\sqrt{s} = 13$ TeV

The CMS Collaboration

Abstract

Results are reported from a search for long-lived exotic particles in proton-proton collision events at a center-of-mass energy of $\sqrt{s} = 13$ TeV delivered by the CERN LHC and collected by the CMS experiment. The data sample, which was recorded during 2015 and 2016, corresponds to an integrated luminosity of 38.5 fb^{-1}. This search uses benchmark signal models in which long-lived exotic particles are pair produced and each decays into two or more quarks, leading to a signal with multiple jets and two displaced vertices composed of many tracks. No events with two well-separated high-track-multiplicity vertices are observed. Upper limits are placed on the pair production cross section as a function of mass and lifetime of the long-lived particle. For masses between 800 and 2600 GeV and mean proper decay lengths between 1 and 40 mm, the analysis excludes cross sections above 0.3 fb at 95% confidence level. In models of R-parity violating supersymmetry in which the long-lived particles are gluinos decaying into multijet final states or top squarks decaying into dijet final states, gluino and top squark masses are excluded below 2200 GeV and 1400 GeV, respectively, for mean proper decay lengths between 0.6 and 80 mm. The results are also applicable to other models in which pair-produced long-lived particles decay into final states with multiple tracks.

1 Introduction

Many theories for physics beyond the standard model (SM) predict the pair production of long-lived particles decaying to final states with two or more jets. Some examples include R-parity violating (RPV) supersymmetry (SUSY) [1], split SUSY [2], hidden valley models [3], and weakly interacting massive particle baryogenesis [4]. Searches for long-lived particles significantly expand the parameter space of physics beyond the SM probed by the experiments at the CERN LHC.

This analysis is sensitive to models of new physics in which pairs of long-lived particles decay to final states with multiple charged particles. We present results for two benchmark signal models, as well as a method for applying the results more generally. The "multijet" benchmark signal is motivated by a minimal flavor violating model of RPV SUSY [5] in which the lightest SUSY particle is a neutralino or gluino, either of which is produced in pairs. The neutralino or gluino is long-lived and decays into a top antiquark and a virtual top squark, and the virtual top squark decays into strange and bottom antiquarks, resulting in a final state with many jets. The "dijet" benchmark signal is a phenomenological model in which pair-produced long-lived top squarks each decay into two down antiquarks, which is also an RPV scenario [6]. The diagrams for the multijet and dijet signal models are shown in Fig. 1.

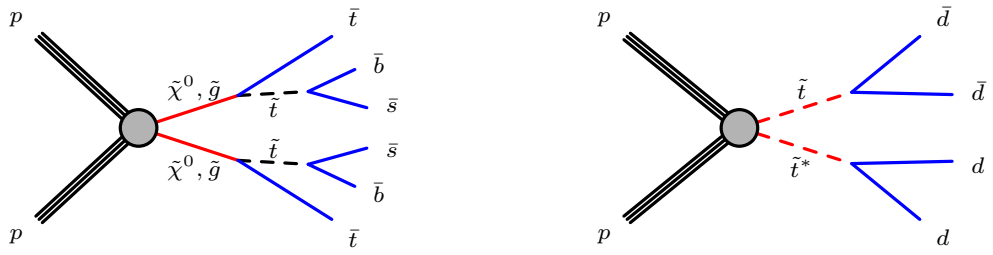

Figure 1: Diagrams for the multijet (left) and dijet (right) benchmark signal models used in this analysis. The long-lived particles are shown in red, and the quarks to which they decay are shown in blue. In the multijet signal model, long-lived neutralinos ($\widetilde{\chi}^0$) or gluinos ($\widetilde{g}$) decay into top, bottom, and strange antiquarks, via a virtual top squark ($\widetilde{t}$). In the dijet signal model, long-lived top squarks decay into two down antiquarks. The charge conjugate processes are also allowed.

The experimental signature of these long-lived exotic particles is a pair of displaced vertices, each consisting of multiple charged-particle trajectories intersecting at a single point. In this analysis, a custom vertex reconstruction algorithm identifies the displaced vertices. We focus on signals with intermediate lifetimes, with mean proper decay lengths from 0.1 to 100 mm, by identifying vertices that are displaced from the beam axis but within the radius of the beam pipe. The signal is distinguished from the SM background based on the separation between the vertices: signal events have two well-separated vertices, while background events are dominated by events with only one displaced vertex, usually close to the beam axis.

The CMS Collaboration searched for displaced vertices in proton-proton (pp) collisions at a center-of-mass energy of $\sqrt{s} = 8$ TeV in 2012 [7]. This analysis is an improved version of the search, using pp collisions collected at $\sqrt{s} = 13$ TeV in 2015 and 2016. A similar analysis was performed by the ATLAS Collaboration [8]. The CMS and ATLAS Collaborations have also searched for displaced jets [9–12], displaced leptons [13, 14], displaced photons [15], and displaced lepton jets [16]. The analysis reported here is sensitive to shorter lifetimes than those probed by previous analyses.

2 The CMS detector

The central feature of the CMS detector is a superconducting solenoid providing a magnetic field of 3.8 T aligned with the proton beam direction. Contained within the field volume of the solenoid are a silicon pixel and strip tracker, a lead tungstate electromagnetic calorimeter, and a brass and scintillator hadron calorimeter. Muon tracking chambers are embedded in the steel flux-return yoke that surrounds the solenoid. A more detailed description of the CMS detector, together with a definition of the coordinate system used and the relevant kinematic variables, can be found in Ref. [17].

The silicon tracker, which is particularly relevant to this analysis, measures the trajectories of charged particles in the range of pseudorapidity, η, up to $|\eta| < 2.5$. For nonisolated particles with transverse momentum, p_T, of 1 to 10 GeV and $|\eta| < 1.4$, the track resolutions are typically 1.5% in p_T, 25–90 μm in the impact parameter in the transverse plane, and 45–150 μm in the impact parameter in the longitudinal direction [18]. Jets are reconstructed from particle-flow [19] candidates using the anti-k_T algorithm [20, 21] with a distance parameter of 0.4.

Events of interest are selected using a two-tiered trigger system [22]. The first level is composed of custom hardware processors, and the second level consists of a farm of processors running a version of the full event reconstruction software optimized for fast processing.

3 Event samples

The data sample used in this analysis corresponds to a total integrated luminosity of 38.5 fb^{-1}, collected in pp collisions at $\sqrt{s} = 13$ TeV in 2015 and 2016. Events are selected using a trigger requiring $H_T > 800$ GeV, where H_T is the scalar sum of the p_T of jets in the event with $p_T > 40$ GeV. In the last data-taking period of 2016, corresponding to 22% of the total integrated luminosity, the higher instantaneous luminosity required an H_T threshold of 900 GeV.

Simulated events are used to model the signal processes. In the multijet and dijet signal models, long-lived particles are produced in pairs; the "multijet" and "dijet" refer to the decay of each long-lived particle. For the multijet signals, the long-lived particle is a neutralino that undergoes a three-body decay into top, bottom, and strange quarks. In this analysis, the final results are the same if the neutralinos are replaced with gluinos. For the dijet signals, the long-lived particle is a top squark that decays into two down antiquarks. Signal samples with varying neutralino or top squark masses M ($300 \leq M \leq 2600$ GeV) and lifetimes τ ($0.1 \leq c\tau \leq 100$ mm) are produced using PYTHIA 8.212 [23] with the NNPDF2.3QED parton distribution functions [24].

Backgrounds arising from SM processes are dominated by multijet and top quark pair production ($\mathrm{t\bar{t}}$) events. The multijet processes include b quark pair production events. The multijet and $\mathrm{t\bar{t}}$ events are simulated using MADGRAPH 5.2.2.2 [25] with the NNPDF3.0 parton distribution functions [26], at leading order for the multijet events and at next-to-leading order for the $\mathrm{t\bar{t}}$ events.

For all samples, hadronization, showering, and R-hadron physics are simulated using PYTHIA 8.212. The underlying event tunes used are CUETP8M1 [27] for the signal samples and the multijet background samples, and CUETP8M2T4 [28] for the $\mathrm{t\bar{t}}$ samples. The detector response for all simulated samples is modeled using a GEANT4-based simulation [29] of the CMS detector. The effects of additional pp interactions per bunch crossing ("pileup") are included by overlaying additional simulated minimum-bias events, such that the resulting distribution of the number of interactions matches that observed in the experiment.

4 Event preselection

For an event to be selected for further analysis, it must have at least four jets, each with $p_{\mathrm{T}} > 20\,\mathrm{GeV}$ and $|\eta| < 2.5$. Since the final states for the signal models considered all have at least four quarks, this requirement has little impact on signal events but is useful for suppressing background.

To ensure that the efficiency of the H_{T} trigger is well understood, a stricter requirement of $H_{\mathrm{T}} > 1000\,\mathrm{GeV}$ is applied offline, where H_{T} is the scalar sum of the p_{T} of jets with $p_{\mathrm{T}} > 40\,\mathrm{GeV}$, matching the trigger jet definition. For events with at least four jets and $H_{\mathrm{T}} > 1000\,\mathrm{GeV}$, the trigger efficiency, determined using events satisfying a single-muon trigger, is $(99 \pm 1)\%$.

5 Vertex reconstruction and selection

Displaced vertices are reconstructed from tracks in the silicon tracker. These tracks are required to have $p_{\mathrm{T}} > 1\,\mathrm{GeV}$; measurements in at least two layers of the pixel detector, including one in the innermost layer; measurements in at least six layers of the strip detector if $|\eta| < 2$, or in at least seven layers if $|\eta| \geq 2$; and significance of the impact parameter with respect to the beam axis measured in the x-y plane (the magnitude of the impact parameter divided by its uncertainty, referred to as $|d_{xy}|/\sigma_{d_{xy}}$) of at least 4. The first three criteria are track quality requirements, imposed in order to select tracks with small impact parameter uncertainties. The requirement on $|d_{xy}|/\sigma_{d_{xy}}$ favors vertices that are displaced from the beam axis.

The vertex reconstruction algorithm forms seed vertices from all pairs of tracks satisfying the track selection criteria, and then merges them iteratively until no track is used more than once. A set of tracks is considered to be a vertex if a fit with the Kalman filter approach [30] has a χ^2 per degree of freedom (χ^2/dof) that is less than 5. For each pair of vertices that shares a track, the vertices are merged if the three-dimensional distance between the vertices is less than 4 times the uncertainty in that distance and the fit has $\chi^2/\mathrm{dof} < 5$. Otherwise, the shared track is assigned to one of the vertices depending on the value of its three-dimensional impact parameter significance with respect to each of the vertices: if both values are less than 1.5, the shared track is assigned to the vertex that has more tracks already; if either value is greater than 5, the shared track is dropped from that vertex; otherwise, the shared track is assigned to the vertex with respect to which it has a smaller impact parameter significance. If a track is removed from a vertex, that vertex is refit, and if the fit satisfies the requirement of $\chi^2/\mathrm{dof} < 5$, the old vertex is replaced with the new one; otherwise it is dropped entirely.

This procedure produces multiple vertices per event, only some of which are signal-like. In order to select vertices with high quality, we impose additional requirements. Each vertex is required to have at least five tracks; distance from the detector origin measured in the x-y plane of less than 20 mm, to avoid vertices from interactions in the beam pipe or detector material; distance from the beam axis measured in the x-y plane, defined as d_{BV}, of at least 0.1 mm, to suppress displaced primary vertices; and uncertainty in d_{BV} of less than 25 μm, to select only well-reconstructed vertices.

Since signal events contain a pair of long-lived particles, we require events to have two or more vertices satisfying the above requirements. The signal region is composed of these two-vertex events. Simulation predicts there is on the order of 1 background event in the signal region for $38.5\,\mathrm{fb}^{-1}$ of data. However, the possibility of a signal relies on an accurate determination of the background, and for this we rely on data.

The vertex selection requires each vertex to have five or more tracks, but events with vertices

with three or four tracks provide valuable control samples. These control samples, which are used to test the background prediction, have a factor of 10–100 more background events than in the signal region and negligible signal contamination. Simulation studies show that events containing 3-track, 4-track, and $\geq$5-track vertices have similar distributions of event variables, such as H_{T}, number of jets, and quark flavor composition, as well as vertex variables, such as d_{BV}, uncertainty in d_{BV}, and angular separation between tracks.

6 Search strategy

The signal is discriminated from the SM background using the distance between the two vertices in the x-y plane, which is defined as d_{VV}. In signal events, the two long-lived particles are emitted approximately back-to-back, leading to large separations. We fit the distribution of d_{VV} to extract the signal.

If an event has more than two vertices, the two vertices with the highest number of tracks are selected for the d_{VV} calculation. In the case in which two vertices have the same number of tracks, the vertex with the higher mass is chosen, where the mass is reconstructed using the momenta of the tracks associated with the vertex, assuming that the particles associated with the tracks have the charged pion mass.

The signal d_{VV} templates are taken directly from simulation, with a distinct template for each signal mass and lifetime. The background template is constructed from data, as described in Section 7. Figure 2 shows examples of the d_{VV} distribution for simulated multijet signals with $M = 800\,\mathrm{GeV}$ and production cross section 1 fb, with the background template overlaid. The distributions depend primarily on the signal lifetime; those for other signal masses and for the dijet signals are similar. The small peaks at low values of d_{VV} are due to the case in which the two vertices are reconstructed from the same long-lived particle, with the effect being larger for the multijet signals.

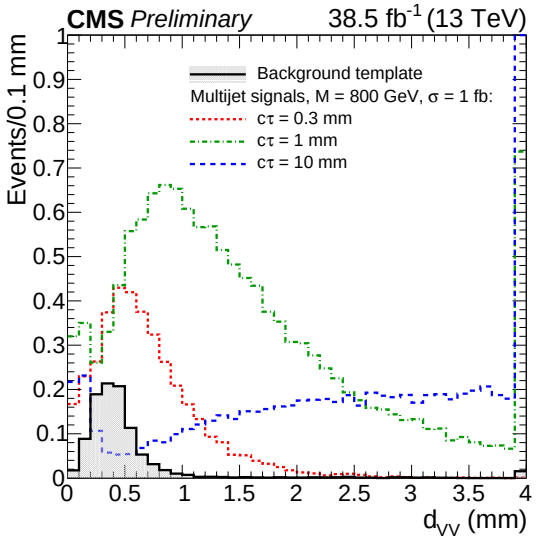

Figure 2: Distribution of the x-y distance between the vertices, d_{VV}, for simulated multijet signals with $M = 800\,\mathrm{GeV}$, production cross section 1 fb, and $c\tau = 0.3$, 1, and 10 mm, with the background template overlaid. All vertex and event selection criteria have been applied. The last bin includes the overflow events.

In the signal extraction procedure, the d_{VV} distribution is broken into three bins: 0–0.4 mm, 0.4–

0.7 mm, and 0.7–40 mm. The two bins with $d_{VV} > 0.4$ mm have low background. This division maximizes the signal significance for scenarios with intermediate and long lifetimes.

Figure 3 shows the signal efficiency as a function of signal mass and lifetime in the region $d_{VV} > 0.4$ mm. The signal efficiency increases with increasing mass because the events are more likely to satisfy the H_T trigger requirement. As lifetime increases, the signal efficiency initially increases because of better separation from the beam axis, but then starts to decreases where the lifetime is so long that decays occur more often beyond the fiducial limit at the beam pipe. The efficiency is above 10% for $c\tau > 0.4$ mm and $M > 800$ GeV.

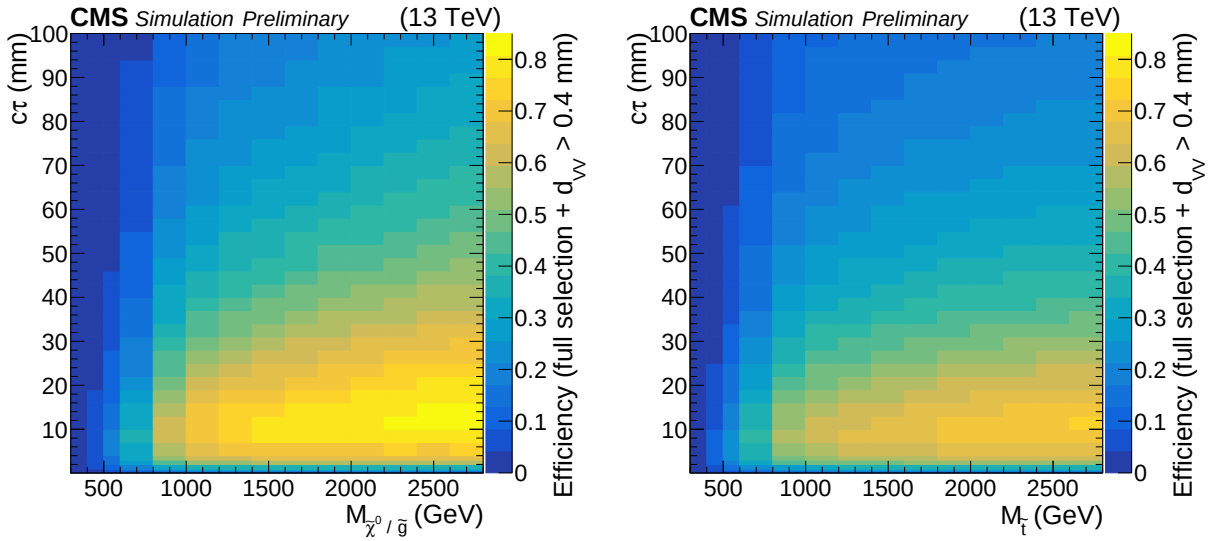

Figure 3: Signal efficiency as a function of signal mass and lifetime, for the multijet signal samples (left) and the dijet signal samples (right). All vertex and event selection criteria have been applied, as well as the requirement $d_{VV} > 0.4$ mm.

7 Background template

Displaced vertices in background events arise from one or more misreconstructed tracks overlapping with other tracks. These events are dominated by multijet and $t\bar{t}$ processes. Background events with two vertices are primarily random coincidences of independently misreconstructed vertices. Accordingly, we construct the two-vertex background template, denoted by d_{VV}^{C}, by combining information from events in data that have exactly one vertex. There are approximately 1000 times more events with only one vertex than there are with two or more vertices, consistently for 3-track, 4-track, and $\geq$5-track vertices. Table 1 lists the number of events in each of the event categories.

Table 1: Event yields in data. The "one-vertex" events have exactly one vertex with the specified number of tracks, and the "two-vertex" events have two or more vertices each with the specified number of tracks. The control samples are composed of the events with 3-track and 4-track vertices, the background template is constructed using the $\geq$5-track one-vertex events, and the signal region is composed of the $\geq$5-track two-vertex events.

Event category	3-track	4-track × 3-track	4-track	$\geq$5-track
one-vertex	109090	—	11923	1183
two-vertex	478	99	7	1

Each entry in the d_{VV}^{C} template is calculated from two values of d_{BV} and a value of $\Delta\phi_{VV}$, where d_{BV} is the x-y distance from the beam axis to one vertex, and $\Delta\phi_{VV}$ is the azimuthal angle between the two vertices. The template also includes corrections for the merging of nearby vertices in the vertex reconstruction algorithm and for possible correlations between individual vertices in background events with pairs of b quarks. The following paragraphs describe each of the inputs to the d_{VV}^{C} template construction method.

The d_{BV} values are sampled from the distribution shown in Fig. 4 for the $\geq$5-track one-vertex events in data. The distribution starts at 0.1 mm due to the fiducial requirement to avoid primary vertices, and falls off exponentially. Signal contamination in the one-vertex sample is negligible for values of the signal cross section that have not been excluded by the previous similar analysis [7].

The statistical uncertainty in the d_{VV}^{C} template, taken as the root-mean-square of yields in an ensemble of simulated pseudo-data sets, depends on the number of entries in the parent d_{BV} distribution. To ensure sufficient sampling of the tail of this distribution, the number of entries in the d_{VV}^{C} template is 20 times the number of one-vertex events.

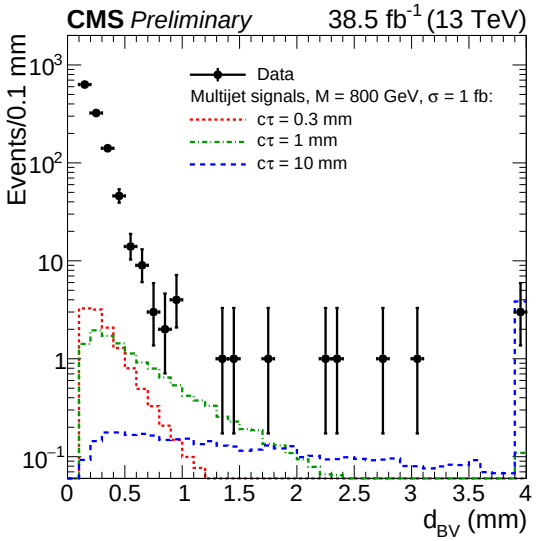

Figure 4: Distribution of d_{BV} in $\geq$5-track one-vertex events for data and simulated multijet signals with $M = 800\,\text{GeV}$, production cross section 1 fb, and $c\tau = 0.3$, 1, and 10 mm. Event preselection and vertex selection criteria have been applied. The last bin includes the overflow events.

Values of $\Delta\phi_{VV}$ are determined from jet directions in data. Since background vertices come from misreconstructed tracks in jets, their position vectors tend to be correlated with jet momentum vectors. The angle between vertex positions can therefore be modeled using the observed distribution of azimuthal angles between pairs of jets, denoted as $\Delta\phi_{JJ}$. The $\Delta\phi_{JJ}$ distribution used for the d_{VV}^{C} construction is taken from the 3-track one-vertex sample, which has a greater number of events than the 4-track and $\geq$5-track one-vertex samples. There are no significant differences in $\Delta\phi_{JJ}$ among these three samples.

To emulate the behavior of the vertex reconstruction algorithm in merging overlapping vertices, the d_{VV}^{C} template is corrected by the survival probability of pairs of vertices as a function of d_{VV}. This efficiency is estimated by counting the number of remaining vertex pairs at each iteration of the vertex reconstruction algorithm. The efficiency correction suppresses small values of d_{VV}^{C}, resulting in a lower yield in the first d_{VV}^{C} bin by a factor of approximately 2.

Pair production of b quarks introduces d_{BV} correlations in two-vertex events that are not accounted for when pairing single vertices at random. This is because the tracks from b quark decays are more likely to satisfy the track $|d_{xy}|/\sigma_{d_{xy}}$ requirement and therefore produce vertices. In simulation, the mean d_{BV} in events with b quarks is higher than in events without b quarks by $47 \pm 1\,\mu$m for 3-track vertices, by $52 \pm 3\,\mu$m for 4-track vertices, and by $50 \pm 6\,\mu$m for $\geq$5-track vertices. The fractions of events with b quarks are consistent across the 3-track, 4-track, and $\geq$5-track vertex samples: approximately 50% in one-vertex events and approximately 78% in two-vertex events. We determine corrections to the $d_{\mathrm{VV}}^{\mathrm{C}}$ template for these d_{BV} correlations by constructing $d_{\mathrm{VV}}^{\mathrm{C}}$ separately for simulated background events with and without generated b quarks, combining the distributions in the ratio of two-vertex events with and without b quarks, and then dividing the resulting distribution by the nominal $d_{\mathrm{VV}}^{\mathrm{C}}$ template. The b quark correction enhances larger values of $d_{\mathrm{VV}}^{\mathrm{C}}$, resulting in a higher yield in the last $d_{\mathrm{VV}}^{\mathrm{C}}$ bin by a factor of 1.6 ± 0.4.

A validation of the background template construction method is shown in the upper left, upper right, and lower left plots in Fig. 5, where $d_{\mathrm{VV}}^{\mathrm{C}}$ is compared to the observed two-vertex d_{VV} distributions in the low-track-multiplicity control samples in data. There is good agreement between the relative $d_{\mathrm{VV}}^{\mathrm{C}}$ and d_{VV} populations in each of the three bins of the final fit. For example, in the 3-track control sample, where this agreement is most stringently tested, the ratios $d_{\mathrm{VV}}^{\mathrm{C}}/d_{\mathrm{VV}}$ are 0.93 ± 0.06 in the 0–0.4 mm bin, 0.97 ± 0.07 in the 0.4–0.7 mm bin, and 1.44 ± 0.20 in the 0.7–40 mm bin.

8 Systematic uncertainties

The signal yield is extracted from a fit of the signal and background templates to the observed d_{VV} distribution. The free parameters are the normalizations of the signal and background templates, subject to the constraint that their combined yield matches the data. The result of the fit relies on the relative yields in the three bins of the templates, but is insensitive to the fine details of the template distributions. This section describes the systematic uncertainties in the background template. It also addresses the systematic uncertainties in the signal efficiencies and templates.

8.1 Systematic uncertainties in signal efficiencies and templates

The signal d_{VV} templates are taken directly from simulation of benchmark models with clearly specified parameters, so the systematic uncertainties arise from biases in the detector and reconstruction simulation. The dominant source of uncertainty is due to the vertex reconstruction efficiency. Smaller effects arise from track resolution, pileup, jet energy scale and resolution, integrated luminosity, and trigger efficiency.

The effect due to the vertex reconstruction efficiency is evaluated by comparing the efficiency in data and simulation to reconstruct signal-like vertices created by displacing tracks artificially. In events passing the preselection requirements (Section 4), we choose some number of light parton and b quark jets that have $p_{\mathrm{T}} > 50\,\mathrm{GeV}$, $|\eta| < 2.5$, and at least four particle-flow candidates. We then artificially displace the tracks associated with those jets as described below.

The magnitude of the displacement vector is sampled from an exponential distribution with scale parameter $c\tau = 10\,\mathrm{mm}$, restricted to values between 0.3 and 20 mm. The direction of the displacement vector is calculated from the vector sum of the momentum of the jets. This direction is smeared to emulate the difference between the vertex displacement direction and jet momentum direction in signal events due to mismeasurements from tracking inefficiency

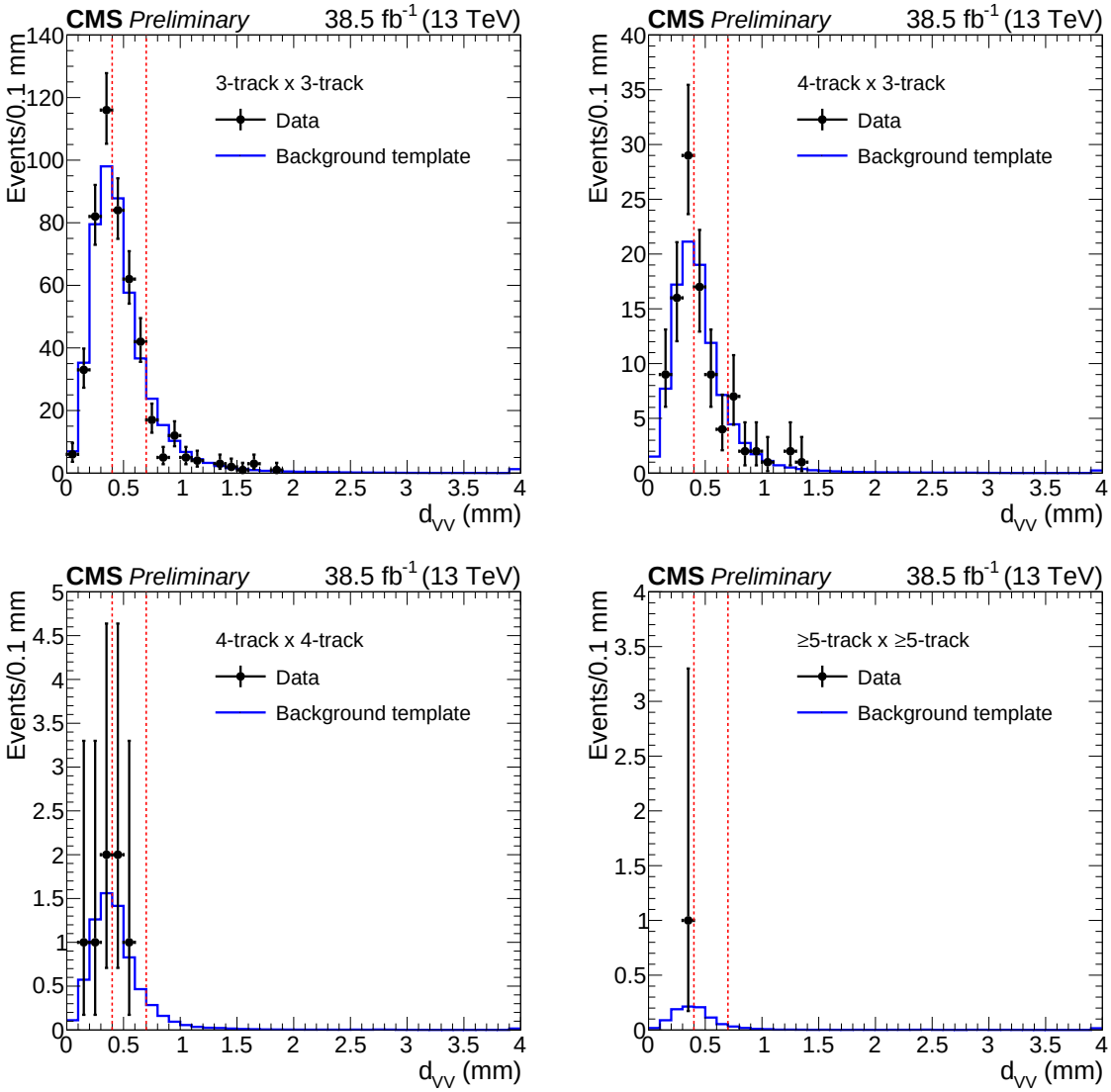

Figure 5: Distribution of the x-y distance between vertices in two-vertex events. The points show the data (d_{VV}), and the solid lines show the background template ($d_{\mathrm{VV}}^{\mathrm{C}}$) normalized to the data, for events with two 3-track vertices (upper left), one 4-track vertex and one 3-track vertex (upper right), two 4-track vertices (lower left), and two $\geq$5-track vertices (lower right). The last bin includes the overflow events. The dotted lines indicate the boundaries between the bins used in the fit.

and missing neutral particles.

The track selection requirements and vertex reconstruction algorithm are applied to the resulting set of tracks. We then evaluate the fraction of events in which a vertex satisfying all vertex selection requirements is reconstructed near the artificial displacement position. This fraction is evaluated for different numbers of displaced light parton or b quark jets. The largest disagreement between data and simulation gives an 11.5% uncertainty per vertex. For two-vertex events, the uncertainty is 23%. Varying the scale parameter of the exponential distribution or the amount that the direction is smeared has negligible effect on the difference between data and simulation.

The difference in vertex reconstruction efficiency between data and simulation could also depend on the magnitude of the artificial displacement. This dependence is found to be small, and the resulting difference in the signal d_{VV} templates has a negligible effect on the signal yield extracted from the fit.

The selection of the tracks used in the vertex reconstruction requires that each track has a value of $|d_{xy}|/\sigma_{d_{xy}}$ of at least 4. The efficiency of this requirement is sensitive to the impact parameter resolution of the tracks. The mean impact parameter uncertainty is 2% larger in data than in simulation. The magnitude of this effect is quantified by tightening the requirement on the transverse impact parameter significance by 2% and evaluating the change in the signal efficiency. The maximum of the effects on the various signal masses and lifetimes, 5%, is taken to be the systematic uncertainty in the signal efficiency. This effect is corrected for in the vertex resolution study discussed earlier.

The uncertainties in the jet energy scale and resolution [31] could affect the total jet energy and change the probability that events satisfy the H_{T} selection. Varying the jet energy scale by one standard deviation results in a change in the signal efficiency of 5% or less for all signal samples, and varying the jet energy resolution by one standard deviation changes the efficiency by 2% or less. We therefore assign these as the corresponding systematic uncertainties in the signal efficiency.

The uncertainty in the integrated luminosity is 2.3% for 2015 [32] and 2.5% for 2016 [33]. The uncertainty in the signal efficiency due to pileup is 2%. The uncertainty in the trigger efficiency is 1%.

Table 2 summarizes the systematic uncertainties in the signal efficiency. We assume there are no correlations among them, so we add them in quadrature to obtain the overall uncertainty.

Table 2: Systematic uncertainties in the signal efficiency. The overall uncertainty is the sum in quadrature of the individual uncertainties.

Systematic effect	Uncertainty (%)
Vertex reconstruction	23
Track resolution	5
Jet energy scale/resolution	5
Integrated luminosity	3
Pileup	2
Trigger efficiency	1
Overall	24

8.2 Systematic uncertainties in the background template

The d_{VV}^{C} background template is constructed from the large sample of events in data with exactly one vertex. Systematic uncertainties in the background template arise from effects that could cause differences between the constructed d_{VV}^{C} distribution and the true d_{VV} distribution of two-vertex background events. The 3-track control sample is used to evaluate the scale of these differences. The deviations from unity of the ratios of the predicted yield in each bin of the d_{VV}^{C} template to the observed yield in the same bin, or the closure, are a measure of the systematic uncertainty. Additional uncertainties arise from effects that could compromise the validity of applying the 3-track control sample to the $\geq$5-track sample.

We check the assumption that closure of the d_{VV}^{C} construction method in 3-track vertices implies closure in $\geq$5-track vertices by varying the inputs to the template construction procedure and evaluating the resulting shifts in the d_{VV}^{C} template. Constructing d_{VV}^{C} involves sampling two values of d_{BV} and an angle between vertices $\Delta\phi_{VV}$, the efficiency to keep pairs of vertices as a function of d_{VV}, and the b quark correction factors, so the main effects are related to these distributions. We take an additional systematic uncertainty for the difference in d_{VV}^{C} predictions due to variations in these distributions from 3-track vertices to $\geq$5-track vertices.

In background template construction, the $\Delta\phi_{VV}$ distribution is modeled using the $\Delta\phi_{JJ}$ distribution in 3-track one-vertex events. The $\Delta\phi_{JJ}$ distribution in $\geq$5-track one-vertex events is indistinguishable from that in 3-track one-vertex events. Potential bias could arise if the distribution of angles between jets and vertices differ for 3-track and $\geq$5-track vertices. Indeed, the vertex displacement directions are less correlated with the direction of jets for $\geq$5-track vertices than for 3-track vertices. To probe the impact, we construct d_{VV}^{C} using a variation of the $\Delta\phi_{VV}$ input in which we assume that the displacement directions are uncorrelated with the jet momentum directions and draw $\Delta\phi_{VV}$ from a uniform distribution. We then assign the fractional difference in the d_{VV}^{C} prediction in each bin as the systematic uncertainty.

The template also depends on the probability that pairs of nearby vertices will both survive the vertex reconstruction algorithm as a function of their separation d_{VV}. The efficiency to merge pairs of vertices is determined from the vertex reconstruction algorithm. To assess the uncertainty due to variations in this efficiency, we use a variation of the algorithm in which the seed vertices are composed of five tracks, rather than the usual two. We then construct a variation of d_{VV}^{C} using the resulting efficiency curve and take the fractional difference in the d_{VV}^{C} prediction in each bin as the systematic uncertainty.

The corrections to the d_{VV}^{C} template that account for d_{BV} correlations due to the pair production of b quarks are derived using the fraction of simulated 3-track two-vertex events with b quarks. This fraction could differ for $\geq$5-track two-vertex events. To assess the related systematic uncertainty, we recompute the b quark corrections using the extreme case in which all two-vertex events contain b quarks, and determine the fractional shifts in the d_{VV}^{C} yields in each bin.

The statistical uncertainties in the b quark corrections are also taken as systematic uncertainties in the template.

The systematic uncertainty in the background template, d_{VV}^{C}, is estimated using a combination of the closure of the construction method in the control sample of 3-track vertices and the difference in effects from 3-track vertices to $\geq$5-track vertices. Table 3 lists the shifts and their statistical uncertainties from these components for each of the three d_{VV} bins. The statistical uncertainties in the shifts take into account the correlation between the default template and the variation. In assessing the overall systematic uncertainty in the background template, we add in quadrature the shifts and their uncertainties, assuming no correlations.

Table 3: Systematic shifts in the background prediction in each d_{VV}^{C} bin arising from varying the construction of the d_{VV}^{C} template. The overall systematic uncertainty is the sum in quadrature of the shifts and their statistical uncertainties, assuming no correlations among the sources.

	Shift (%)		
Systematic effect	0–0.4 mm	0.4–0.7 mm	0.7–40 mm
Closure in 3-track control sample	-7 ± 6	-3 ± 7	$+44 \pm 20$
Difference from 3-track to $\geq$5-track vertices:			
Modeling of $\Delta\phi_{VV}$	$+4 \pm 0$	-5 ± 1	-2 ± 3
Modeling of vertex survival efficiency	$+20 \pm 1$	-19 ± 2	-26 ± 7
Modeling of b quark correction	-11 ± 1	$+9 \pm 2$	$+18 \pm 9$
b quark correction statistical uncertainty	± 3	± 9	± 36
Overall systematic uncertainty	25	25	69

9 Signal extraction and statistical interpretation

To determine the signal yield, we perform binned shape fits of the signal and background templates to the d_{VV} distribution using an extended likelihood method [34].

The background template is constructed from the one-vertex events in data, while the signal templates are produced directly using the d_{VV} distributions from simulation. There is one signal template for each signal model, mass, and lifetime.

The lower right plot in Fig. 5 compares the d_{VV}^{C} and d_{VV} distributions in the signal region. The observed number of events in each bin, along with the predictions from the background-only fit and from example signal models, are listed in Table 4. The background-only fit normalizes the prediction from the d_{VV}^{C} background template to the observed number of two-vertex events. Since there was only one two-vertex event in data, falling in the 0–0.4 mm d_{VV} bin, signal-plus-background fits to the observed distribution with any signal point prefer zero signal yield, which is constrained to be nonnegative in the fit.

Table 4: In $\geq$5-track two-vertex events: for each d_{VV} bin, the predicted background yield from the background-only fit, the observed yield, and the predicted signal yields for simulated multijet signals with $M = 2000$ GeV, production cross section 1 fb, and $c\tau = 0.3$, 1, and 10 mm. The systematic uncertainties in the predicted background yields reflect the fractional systematic uncertainties given in Table 3, and the uncertainties in the predicted signal yields reflect the fractional systematic uncertainty given in Table 2.

			Predicted signal yields		
d_{VV} range	Fitted background yield	Observed	0.3 mm	1 mm	10 mm
0–0.4 mm	$0.51 \pm 0.01\,(\text{stat}) \pm 0.13\,(\text{syst})$	1	2.8 ± 0.7	3.5 ± 0.8	1.0 ± 0.2
0.4–0.7 mm	$0.37 \pm 0.02\,(\text{stat}) \pm 0.09\,(\text{syst})$	0	2.0 ± 0.5	3.7 ± 0.9	0.5 ± 0.1
0.7–40 mm	$0.12 \pm 0.02\,(\text{stat}) \pm 0.08\,(\text{syst})$	0	1.1 ± 0.3	11 ± 3	31 ± 7

Upper limits on the signal cross section are set using a Bayesian technique [35]. A uniform prior is taken for positive values of the signal cross section. The signal event yield is constrained by a log-normal prior with a width of 24%, reflecting the overall uncertainty in the signal efficiency (Table 2). The only assumed shape uncertainty in the signal templates is that due to the finite number of events in the simulation; the uncertainty can be up to 20% for the lower lifetime and mass samples that have small efficiencies. For the uncertainty in the background, log-normal priors are taken for the yield in each bin, with widths given by the fractional uncertainties listed in Table 3.

Figure 6 shows, as a function of lifetime and mass, the observed 95% confidence level (CL) upper limits on the signal cross section times branching fraction squared ($\sigma\mathcal{B}^2$) for both the multijet and dijet signal templates. The expected limits are similar numerically. Exclusion curves are overlaid, assuming gluino and top squark pair production cross sections [36] and 100% branching fraction, for both the observed and expected 95% CL upper limits. The upper limits reflect the signal efficiencies shown in Fig. 3, initially improving as lifetime increases, but worsening at approximately 40 mm due to the fiducial limit at the beam pipe. As an example, for a neutralino with mass of 800 GeV and $c\tau = 1$ mm, the observed 95% CL upper limit on $\sigma\mathcal{B}^2$ is 0.3 fb. Figure 7 shows the upper limits as a function of mass for several values of $c\tau$, and Fig. 8 shows the upper limits as a function of $c\tau$ for several values of the mass.

In Fig. 8, the narrowing of the expected limit bands above $c\tau = 2$ mm is due to the correlation between the signal lifetime and the relative signal yields in the three d_{VV} bins. The low background yield causes the discrete nature of the Poisson distribution to have an effect: the pseudo-data sets used to calculate the distribution of expected limits have a limited number of combinations of yields in each bin. For example, for a simulated multijet signal with $M = 1600$ GeV and $c\tau = 4$ mm, the signal density is almost entirely (>90%) in the last bin. The majority of pseudo-data sets that are different in only the first two bins then have nearly the same expected limit value. The bands widen above $c\tau = 20$ mm with the reappearance of signal density in the first bin due to the effect described in Section 6 in which two vertices are reconstructed from the same long-lived particle, an effect that is larger for the multijet signals.

10 Extending the search to other signal models

This search for displaced vertices applies to other types of long-lived particles decaying to multiple jets. Here we present a generator-level selection that can be used to reinterpret the results of our analysis. For signal models in which there are two long-lived particles, this generator-level selection approximately replicates the reconstruction-level efficiency. The selection is based on the number and momenta of generated jets in the event, the displacements of the long-lived particles, and the momenta of their daughter particles. The generated jets are those clustered from all final-state particles except neutrinos, using the anti-k_{T} algorithm with a distance parameter of 0.4, but are rejected if the fraction of energy from electrons is greater than 0.9 or if the fraction of energy from muons is greater than 0.8. The daughter particles are the u, d, s, c, and b quarks, electrons, muons, and tau leptons from the decay of the long-lived particle, and we consider those with an impact parameter with respect to the origin measured in the x-y plane of at least 0.1 mm. The generated jets and daughter particles are required to satisfy $p_{\mathrm{T}} > 20$ GeV and $|\eta| < 2.5$.

The criteria of the generator-level selection are at least four generated jets; $H_{\mathrm{T}} > 1000$ GeV, where H_{T} is the scalar sum of the p_{T} of generated jets with $p_{\mathrm{T}} > 40$ GeV; for each long-lived particle, distance of the decay point from the origin measured in the x-y plane of between 0.1 and 20 mm, and Σp_{T} of the daughter particles of at least 350 GeV; and distance between the decay points of the long-lived particles measured in the x-y plane of at least 0.4 mm. In calculating the Σp_{T} of the daughter particles, we multiply the p_{T} of b quark daughter particles by a factor of 0.65. This accounts for the lower reconstruction-level efficiency due to the heavy flavor lifetime, which can impede the association of their decay products with the reconstructed vertices.

In the region with $d_{\mathrm{VV}} > 0.4$ mm, there are no observed events. This generator-level selection replicates the reconstruction-level efficiency with a typical accuracy of 20% for a variety of models for which the signal efficiency is high (>10%).

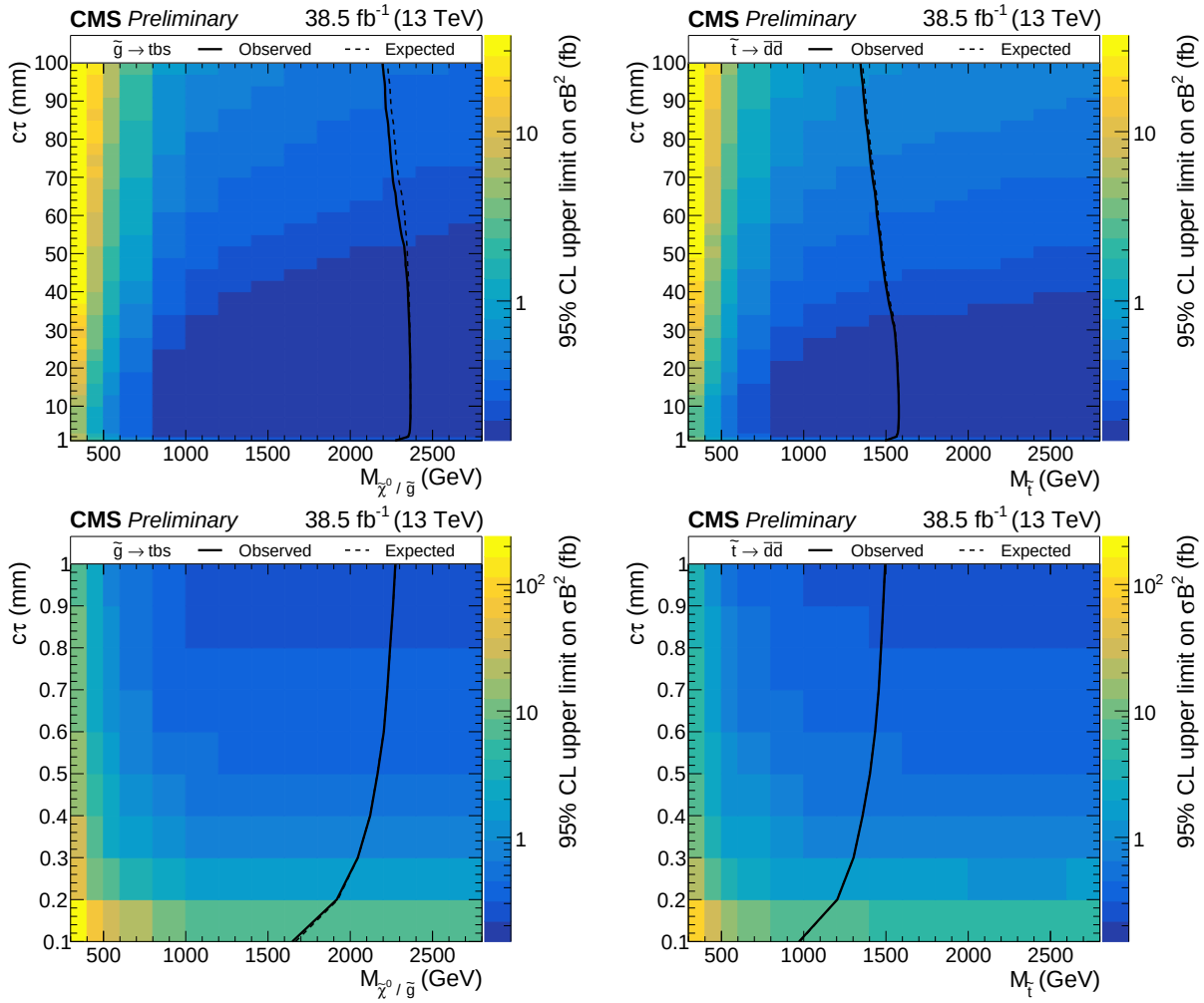

Figure 6: Observed 95% CL upper limits on cross section times branching fraction squared for multijet signals (left) and dijet signals (right) as a function of mass and mean proper decay length. The overlaid mass exclusion curves assume gluino pair production cross sections for the multijet signals and top squark pair production cross sections for the dijet signals. The upper plots span $c\tau$ from 1 to 100 mm, and the lower plots span $c\tau$ from 0.1 to 1 mm.

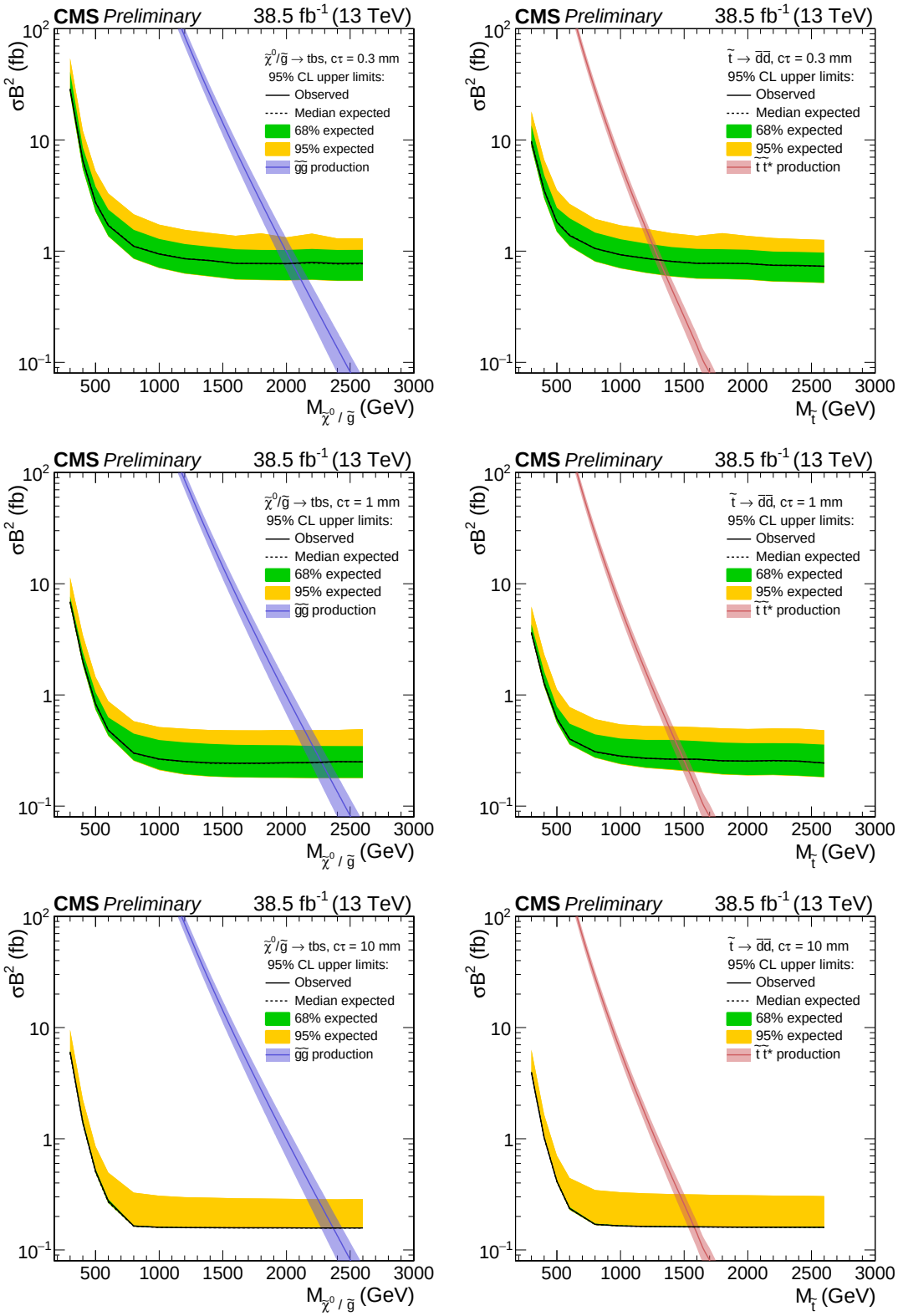

Figure 7: Observed and expected 95% CL upper limits on cross section times branching fraction squared for multijet signals (left) and dijet signals (right), as a function of mass for a fixed $c\tau$ of 0.3 mm (upper), 1 mm (middle), and 10 mm (lower). The gluino pair production cross section is overlaid for the multijet signals, and the top squark pair production cross section is overlaid for the dijet signals. The uncertainty in the theoretical cross sections include those due to the renormalization and factorization scales, and the parton distribution functions.

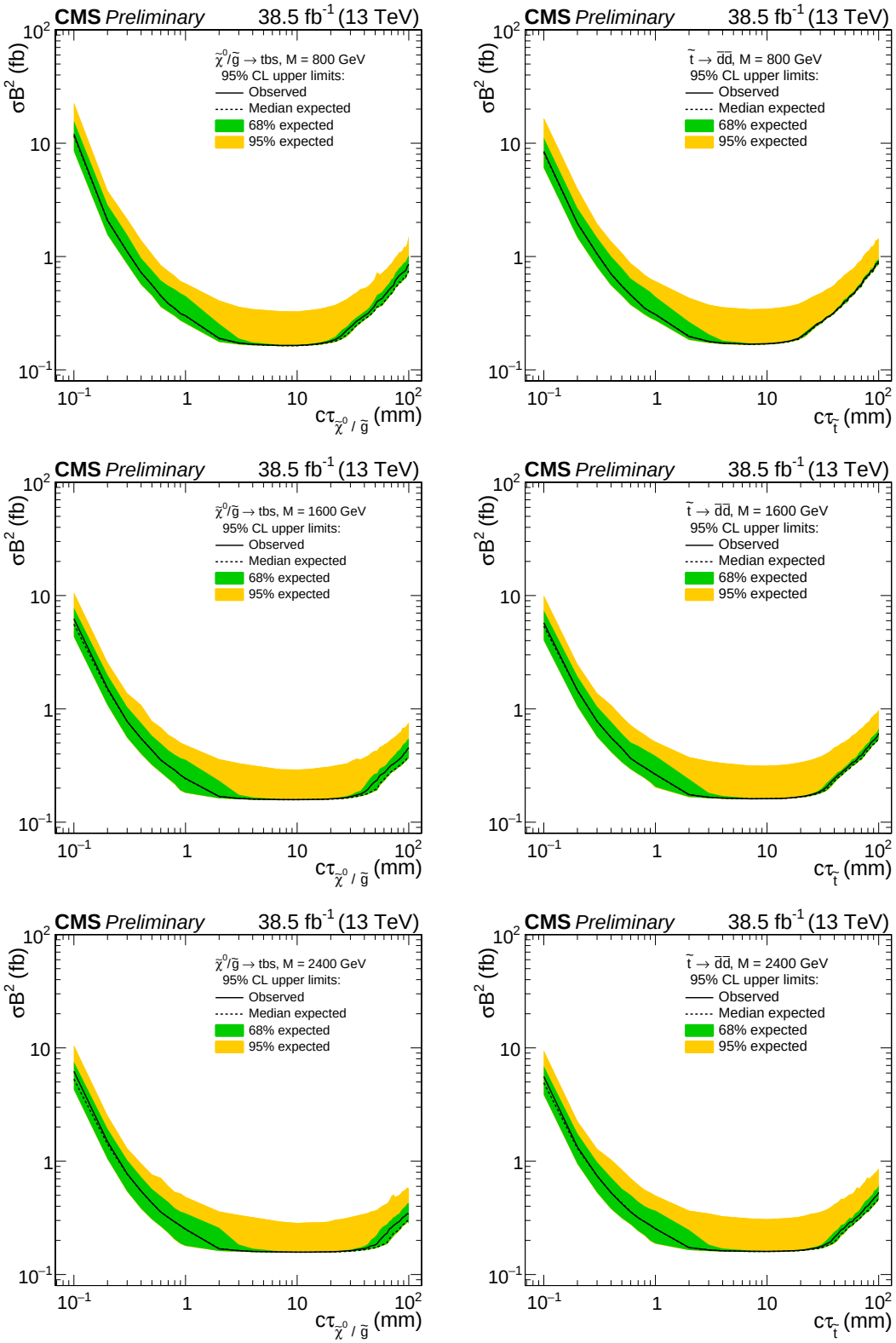

Figure 8: Observed and expected 95% CL upper limits on cross section times branching fraction squared for multijet signals (left) and dijet signals (right), as a function of $c\tau$ for a fixed mass of 800 GeV (upper), 1600 GeV (middle), and 2400 GeV (lower).

11 Summary

A search for long-lived particles decaying into multijet final states is performed using proton-proton collision events collected with the CMS detector at a center-of-mass-energy of $\sqrt{s} = 13\,\text{TeV}$ in 2015 and 2016. The data sample corresponds to an integrated luminosity of $38.5\,\text{fb}^{-1}$. No excess yield above the prediction from standard model processes is observed. At 95% confidence level, the data excludes cross section times branching fraction squared above approximately 0.3 fb for long-lived particles with mass between 800 and 2600 GeV and mean proper decay length between 1 and 40 mm. Assuming gluino and top squark pair production cross sections [36], gluino masses below 2200 GeV and top squark masses below 1400 GeV are excluded for mean proper decay lengths between 0.6 and 80 mm. While the search specifically addresses two models of R-parity violating supersymmetry, the results are relevant to other models in which long-lived particles decay to final states with multiple tracks. Improved techniques, increased center-of-mass energy, and higher integrated luminosity relative to the 8 TeV search [7] lead to more restrictive bounds on long-lived particle pair production cross sections and the mass of the gluino, and place new exclusions on the mass of the top squark.

Acknowledgments

We congratulate our colleagues in the CERN accelerator departments for the excellent performance of the LHC and thank the technical and administrative staffs at CERN and at other CMS institutes for their contributions to the success of the CMS effort. In addition, we gratefully acknowledge the computing centers and personnel of the Worldwide LHC Computing Grid for delivering so effectively the computing infrastructure essential to our analyses. Finally, we acknowledge the enduring support for the construction and operation of the LHC and the CMS detector provided by the following funding agencies: BMWFW and FWF (Austria); FNRS and FWO (Belgium); CNPq, CAPES, FAPERJ, and FAPESP (Brazil); MES (Bulgaria); CERN; CAS, MoST, and NSFC (China); COLCIENCIAS (Colombia); MSES and CSF (Croatia); RPF (Cyprus); SENESCYT (Ecuador); MoER, ERC IUT, and ERDF (Estonia); Academy of Finland, MEC, and HIP (Finland); CEA and CNRS/IN2P3 (France); BMBF, DFG, and HGF (Germany); GSRT (Greece); NKFIA (Hungary); DAE and DST (India); IPM (Iran); SFI (Ireland); INFN (Italy); MSIP and NRF (Republic of Korea); LAS (Lithuania); MOE and UM (Malaysia); BUAP, CINVESTAV, CONACYT, LNS, SEP, and UASLP-FAI (Mexico); MBIE (New Zealand); PAEC (Pakistan); MSHE and NSC (Poland); FCT (Portugal); JINR (Dubna); MON, RosAtom, RAS and RFBR (Russia); MESTD (Serbia); SEIDI, CPAN, PCTI and FEDER (Spain); Swiss Funding Agencies (Switzerland); MST (Taipei); ThEPCenter, IPST, STAR, and NSTDA (Thailand); TUBITAK and TAEK (Turkey); NASU and SFFR (Ukraine); STFC (United Kingdom); DOE and NSF (USA).

Individuals have received support from the Marie-Curie program and the European Research Council and Horizon 2020 Grant, contract No. 675440 (European Union); the Leventis Foundation; the A. P. Sloan Foundation; the Alexander von Humboldt Foundation; the Belgian Federal Science Policy Office; the Fonds pour la Formation à la Recherche dans l'Industrie et dans l'Agriculture (FRIA-Belgium); the Agentschap voor Innovatie door Wetenschap en Technologie (IWT-Belgium); the F.R.S.-FNRS and FWO (Belgium) under the "Excellence of Science - EOS" - be.h project n. 30820817; the Ministry of Education, Youth and Sports (MEYS) of the Czech Republic; the Lendület ("Momentum") Programme and the János Bolyai Research Scholarship of the Hungarian Academy of Sciences, the New National Excellence Program ÚNKP, the NKFIA research grants 123842, 123959, 124845, 124850 and 125105 (Hungary); the Council of Science and Industrial Research, India; the HOMING PLUS program of the Foun-

dation for Polish Science, cofinanced from European Union, Regional Development Fund, the Mobility Plus program of the Ministry of Science and Higher Education, the National Science Center (Poland), contracts Harmonia 2014/14/M/ST2/00428, Opus 2014/13/B/ST2/02543, 2014/15/B/ST2/03998, and 2015/19/B/ST2/02861, Sonata-bis 2012/07/E/ST2/01406; the National Priorities Research Program by Qatar National Research Fund; the Programa Estatal de Fomento de la Investigación Científica y Técnica de Excelencia María de Maeztu, grant MDM-2015-0509 and the Programa Severo Ochoa del Principado de Asturias; the Thalis and Aristeia programs cofinanced by EU-ESF and the Greek NSRF; the Rachadapisek Sompot Fund for Postdoctoral Fellowship, Chulalongkorn University and the Chulalongkorn Academic into Its 2nd Century Project Advancement Project (Thailand); the Welch Foundation, contract C-1845; and the Weston Havens Foundation (USA).

References

[1] R. Barbier et al., "*R*-parity violating supersymmetry", *Phys. Rept.* **420** (2005) 1, doi:10.1016/j.physrep.2005.08.006, arXiv:hep-ph/0406039.

[2] J. L. Hewett, B. Lillie, M. Masip, and T. G. Rizzo, "Signatures of long-lived gluinos in split supersymmetry", *JHEP* **09** (2004) 070, doi:10.1088/1126-6708/2004/09/070, arXiv:hep-ph/0408248.

[3] M. J. Strassler and K. M. Zurek, "Echoes of a hidden valley at hadron colliders", *Phys. Lett. B* **651** (2007) 374, doi:10.1016/j.physletb.2007.06.055, arXiv:hep-ph/0604261.

[4] Y. Cui and B. Shuve, "Probing baryogenesis with displaced vertices at the LHC", *JHEP* **02** (2015) 049, doi:10.1007/JHEP02(2015)049, arXiv:1409.6729.

[5] C. Csáki, Y. Grossman, and B. Heidenreich, "Minimal flavor violation supersymmetry: a natural theory for *R*-parity violation", *Phys. Rev. D* **85** (2012) 095009, doi:10.1103/PhysRevD.85.095009, arXiv:1111.1239.

[6] C. Csáki et al., "Phenomenology of a long-lived LSP with *R*-parity violation", *JHEP* **08** (2015) 016, doi:10.1007/JHEP08(2015)016, arXiv:1505.00784.

[7] CMS Collaboration, "Search for *R*-parity violating supersymmetry with displaced vertices in proton-proton collisions at $\sqrt{s} = 8\,\text{TeV}$", *Phys. Rev. D* **95** (2017) 012009, doi:10.1103/PhysRevD.95.012009, arXiv:1610.05133.

[8] ATLAS Collaboration, "Search for long-lived, massive particles in events with displaced vertices and missing transverse momentum in $\sqrt{s} = 13\,\text{TeV}$ pp collisions with the ATLAS detector", *Phys. Rev. D* **97** (2018) 052012, doi:10.1103/PhysRevD.97.052012, arXiv:1710.04901.

[9] CMS Collaboration, "Search for long-lived neutral particles decaying to quark-antiquark pairs in proton-proton collisions at $\sqrt{s} = 8\,\text{TeV}$", *Phys. Rev. D* **91** (2015) 012007, doi:10.1103/PhysRevD.91.012007, arXiv:1411.6530.

[10] ATLAS Collaboration, "Search for pair-produced long-lived neutral particles decaying in the ATLAS hadronic calorimeter in pp collisions at $\sqrt{s} = 8\,\text{TeV}$", *Phys. Lett. B* **743** (2015) 15, doi:10.1016/j.physletb.2015.02.015, arXiv:1501.04020.

[11] ATLAS Collaboration, "Search for long-lived, weakly interacting particles that decay to displaced hadronic jets in proton-proton collisions at $\sqrt{s} = 8$ TeV with the ATLAS detector", *Phys. Rev. D* **92** (2015) 012010, doi:10.1103/PhysRevD.92.012010, arXiv:1504.03634.

[12] CMS Collaboration, "Search for new long-lived particles at $\sqrt{s} = 13$ TeV", *Phys. Lett. B* **780** (2018) 432, doi:10.1016/j.physletb.2018.03.019, arXiv:1711.09120.

[13] CMS Collaboration, "Search for displaced supersymmetry in events with an electron and a muon with large impact parameters", *Phys. Rev. Lett.* **114** (2015) 061801, doi:10.1103/PhysRevLett.114.061801, arXiv:1409.4789.

[14] CMS Collaboration, "Search for long-lived particles that decay into final states containing two electrons or two muons in proton-proton collisions at $\sqrt{s} = 8$ TeV", *Phys. Rev. D* **91** (2015) 052012, doi:10.1103/PhysRevD.91.052012, arXiv:1411.6977.

[15] ATLAS Collaboration, "Search for nonpointing and delayed photons in the diphoton and missing transverse momentum final state in 8 TeV pp collisions at the LHC using the ATLAS detector", *Phys. Rev. D* **90** (2014) 112005, doi:10.1103/PhysRevD.90.112005, arXiv:1409.5542.

[16] ATLAS Collaboration, "Search for long-lived neutral particles decaying into lepton jets in proton-proton collisions at $\sqrt{s} = 8$ TeV with the ATLAS detector", *JHEP* **11** (2014) 088, doi:10.1007/JHEP11(2014)088, arXiv:1409.0746.

[17] CMS Collaboration, "The CMS experiment at the CERN LHC", *JINST* **3** (2008) S08004, doi:10.1088/1748-0221/3/08/S08004.

[18] CMS Collaboration, "Description and performance of track and primary-vertex reconstruction with the CMS tracker", *JINST* **9** (2014) P10009, doi:10.1088/1748-0221/9/10/P10009, arXiv:1405.6569.

[19] CMS Collaboration, "Particle-flow reconstruction and global event description with the CMS detector", *JINST* **12** (2017) P10003, doi:10.1088/1748-0221/12/10/P10003, arXiv:1706.04965.

[20] M. Cacciari, G. P. Salam, and G. Soyez, "The anti-k_t jet clustering algorithm", *JHEP* **04** (2008) 063, doi:10.1088/1126-6708/2008/04/063, arXiv:0802.1189.

[21] M. Cacciari, G. P. Salam, and G. Soyez, "FastJet user manual", *Eur. Phys. J. C* **72** (2012) 1896, doi:10.1140/epjc/s10052-012-1896-2, arXiv:1111.6097.

[22] CMS Collaboration, "The CMS trigger system", *JINST* **12** (2017) P01020, doi:10.1088/1748-0221/12/01/P01020, arXiv:1609.02366.

[23] T. Sjöstrand et al., "An introduction to PYTHIA 8.2", *Comput. Phys. Commun.* **191** (2015) 159, doi:10.1016/j.cpc.2015.01.024, arXiv:1410.3012.

[24] NNPDF Collaboration, "Parton distributions with QED corrections", *Nucl. Phys. B* **877** (2013) 290, doi:10.1016/j.nuclphysb.2013.10.010, arXiv:1308.0598.

[25] J. Alwall et al., "The automated computation of tree-level and next-to-leading order differential cross sections, and their matching to parton shower simulations", *JHEP* **07** (2014) 079, doi:10.1007/JHEP07(2014)079, arXiv:1405.0301.

[26] NNPDF Collaboration, "Parton distributions for the LHC Run II", *JHEP* **04** (2015) 040, doi:10.1007/JHEP04(2015)040, arXiv:1410.8849.

[27] CMS Collaboration, "Event generator tunes obtained from underlying event and multiparton scattering measurements", *Eur. Phys. J. C* **76** (2016) 155, doi:10.1140/epjc/s10052-016-3988-x, arXiv:1512.00815.

[28] CMS Collaboration, "Investigations of the impact of the parton shower tuning in Pythia 8 in the modelling of $\mathrm{t\bar{t}}$ at $\sqrt{s} = 8$ and 13 TeV", CMS Physics Analysis Summary CMS-PAS-TOP-16-021, 2016.

[29] GEANT4 Collaboration, "GEANT4—a simulation toolkit", *Nucl. Instrum. Meth. A* **506** (2003) 250, doi:10.1016/S0168-9002(03)01368-8.

[30] R. Frühwirth, "Application of Kalman filtering to track and vertex fitting", *Nucl. Instrum. Meth. A* **262** (1987) 444, doi:10.1016/0168-9002(87)90887-4.

[31] CMS Collaboration, "Jet energy scale and resolution in the CMS experiment in pp collisions at 8 TeV", *JINST* **12** (2017) P02014, doi:10.1088/1748-0221/12/02/P02014, arXiv:1607.03663.

[32] CMS Collaboration, "CMS luminosity measurement for the 2015 data-taking period", CMS Physics Analysis Summary CMS-PAS-LUM-15-001, 2017.

[33] CMS Collaboration, "CMS luminosity measurements for the 2016 data-taking period", CMS Physics Analysis Summary CMS-PAS-LUM-17-001, 2017.

[34] R. J. Barlow, "Extended maximum likelihood", *Nucl. Instrum. Meth. A* **297** (1990) 496, doi:10.1016/0168-9002(90)91334-8.

[35] G. Cowan, "Statistics", Ch. 39 in Particle Data Group, C. Patrignani et al., "Review of particle physics", *Chin. Phys. C* **40** (2016) 100001, doi:10.1088/1674-1137/40/10/100001.

[36] C. Borschensky et al., "Squark and gluino production cross sections in pp collisions at $\sqrt{s} = 13$, 14, 33 and 100 TeV", *Eur. Phys. J. C* **74** (2014) 3174, doi:10.1140/epjc/s10052-014-3174-y, arXiv:1407.5066.